THE JOURNAL OF BIOLOGICAL CHEMISTRY VOL. 291, NO. 46, pp. 24148–24159, November 11, 2016

Prohibitin 1 Regulates the H19-Igf2 Axis and Proliferation in Hepatocytes*[S]

Received for publication, June 16, 2016, and in revised form, September 26, 2016 Published, JBC Papers in Press, September 29, 2016, DOI 10.1074/jbc.M116.744045

Komal Ramani[‡1], **Nirmala Mavila**[‡1], **Kwang Suk Ko**[§], **José M. Mato**[¶], **and Shelly C. Lu**[‡2]

From the [‡]*Division of Gastroenterology and Hepatology, Cedars-Sinai Medical Center, Los Angeles, California 90048, the* [§]*Department of Nutritional Science and Food Management, the College of Health Science, Ewha Womans University, Seoul 03760, Korea, and the* [¶]*CIC bioGUNE, Centro de Investigación Biomédica en Red de Enfermedades Hepáticas y Digestivas (Ciberehd), Technology Park of Bizkaia, 48160 Derio, Bizkaia, Spain*

Edited by Xiao-Fan Wang

Prohibitin 1 (PHB1) is a mitochondrial chaperone that regulates cell growth. *Phb1* knock-out mice exhibit liver injury and hepatocellular carcinoma (HCC). *Phb1* knock-out livers show induction of tumor growth-associated genes, *H19* and insulin-like growth factor 2 (*Igf2*). These genes are controlled by the imprinting control region (ICR) containing CCCTC-binding transcription factor (CTCF)-binding sites. Because *Phb1* knock-out mice exhibited induction of *H19* and *Igf2*, we hypothesized that PHB1-mediated regulation of the *H19-Igf2* axis might control cell proliferation in normal hepatocytes. *H19* and *Igf2* were induced (8–20-fold) in 3-week-old *Phb1* knock-out livers, in *Phb1* siRNA-treated AML12 hepatocytes (2-fold), and HCC cell lines when compared with control. *Phb1* knockdown lowered CTCF protein in AML12 by ~30% when compared with control. CTCF overexpression lowered basal *H19* and *Igf2* expression by 30% and suppressed *Phb1* knockdown-mediated induction of these genes. CTCF and PHB1 co-immunoprecipitated and co-localized on the ICR element, and *Phb1* knockdown lowered CTCF ICR binding activity. The results suggest that PHB1 and CTCF cooperation may control the *H19-Igf2* axis. Human HCC tissues with high levels of *H19* and *IGF2* exhibited a 40–50% reduction in *PHB1* and *CTCF* expression and their ICR binding activity. Silencing *Phb1* or overexpressing *H19* in the mouse HCC cell line, SAMe-D, induced cell growth. Blocking *H19* induction prevented *Phb1* knockdown-mediated growth, whereas *H19* overexpression had the reverse effect. Interestingly *H19* silencing induced PHB1 expression. Taken together, our results demonstrate that the *H19-Igf2* axis is negatively regulated by CTCF-PHB1 cooperation and that *H19* is involved in modulating the growth-suppressive effect of PHB1 in the liver.

Prohibitin 1 (PHB1) is a ubiquitously expressed mitochondrial chaperone protein with diverse functions (1). Membrane-bound PHB1 regulates downstream signaling pathways, whereas mitochondrial and nuclear PHB1 regulates apoptosis, transcriptional activation, and cell cycle, indicating the important link between its cellular localization and function (2, 3) Studies have demonstrated that PHB1 protects cells from oxidative stress and maintains the functional integrity of the mitochondria (2, 4, 5). Nuclear PHB1 co-localizes with p53, E2F1, and retinoblastoma protein (6–8). In breast cancer and B-cell lymphoma cell lines, *Phb1* overexpression induces p53 transcriptional activity, whereas it represses E2F1-mediated transcription via its interaction with the retinoblastoma protein (3, 9). Despite this strong evidence of anti-tumorigenic properties of PHB1, a number of studies have indicated the pro-tumorigenic effects of PHB1. Membrane-associated PHB1 interacts with C-Raf and is indispensable for the activation of the Ras-Raf-MEK-ERK signaling pathway, which may modulate cancer cell survival and migration (10). Also, *Phb1* is up-regulated in many cancers such as breast, prostate, ovarian, lung, bladder, thyroid, and gastric cancer (9). One of the reasons for this induction is thought to be the presence of binding sites for c-Myc in the *Phb1* promoter (9). However, a direct effect of c-Myc on *Phb1* transcription has not been reported so far. It is possible that the controversial role of *Phb1* in tumorigenesis and cell survival may be explained by cell type-specific mechanisms, subcellular localization, and even protein post-translational modifications such as phosphorylation (10).

PHB1 was originally cloned from regenerating livers where its expression was nearly absent shortly after two-thirds partial hepatectomy and hence thought to be a tumor suppressor (11). To examine molecular mechanisms of action of *Phb1* in the liver, we previously developed the liver-specific *Phb1* knock-out (*Phb1* KO) mouse model (12). *Phb1* KO mice livers develop severe oxidative stress, fibrosis, and liver cancer (12). Microarray analysis of *Phb1* KO mice livers revealed a significant up-regulation of the long noncoding RNA, *H19* and insulin-like growth factor 2 (*Igf2*) genes (12). These genes are part of a well characterized cluster that contains the paternally expressed *Igf2* and maternally expressed *H19*. Both genes share enhancers and are asynchronously regulated at a site called the imprinting control region (ICR)[3] (13). Loss of imprinting of both *Igf2* and

* This work was supported by National Institutes of Health Grant R01CA172086 (to S. C. L., H. P. Yang, and J. M. M.), Plan Nacional of I+D SAF 2014-52097R, and Departamento de Educación del Gobierno Vasco (to J. M. M.), and National Research Foundation of Korea NRF-2012R1A1A1012261 (to K. S. K.). The authors declare that they have no conflicts of interest with the contents of this article. The content is solely the responsibility of the authors and does not necessarily represent the official views of the National Institutes of Health.

[S] This article contains supplemental Figs. 1–5.

[1] These two authors should be regarded as joint first authors.

[2] To whom correspondence should be addressed. Tel.: 310-423-5692; E-mail: shelly.lu@cshs.org.

[3] The abbreviations used are: ICR, imprinting control region; HCC, hepatocellular carcinoma; CTCF, CCCTC-binding transcription factor; FL, floxed; EV, empty vector.

H19 has been observed in hepatocellular carcinoma (HCC) tissues and cell lines (14, 15). *Igf2* is frequently activated in human cancers and in experimental liver carcinogenesis and is known to promote HCC growth (16, 17). *H19* expression has been positively correlated with hepatocyte proliferation after partial hepatectomy in rodents and with tumor cell growth (18, 19). Although *H19* expression positively correlates with growth, the underlying mechanisms by which *H19* may contribute to liver cell proliferation and HCC are not clearly established.

CCCTC-binding factor (CTCF) is a ubiquitous transcription factor that acts as both a transcriptional activator and a repressor. On the ICR, it controls allele-specific *H19* and *Igf2* expression by a DNA methylation-dependent mechanism. CTCF binding to the ICR element negatively regulates *Igf2* expression on the maternal allele by blocking the access of *Igf2* promoter to a downstream enhancer sequence (13). However, the expression of *H19* is retained on the maternal allele. On the paternal allele, the ICR becomes methylated, thereby preventing *H19* expression. However, this methylated ICR prevents CTCF from binding and hence allows *Igf2* expression from a downstream enhancer (13, 20). To our knowledge, CTCF has not been reported to regulate *H19* expression.

The current study was undertaken to investigate the molecular mechanism by which PHB1 may regulate the expression of *H19* and *Igf2* and whether this axis contributes to the effect of PHB1 on liver cell proliferation. Our data demonstrate for the first time that PHB1 negatively regulates *H19* and *Igf2* levels by acting as a co-repressor with CTCF on the ICR. Depletion of PHB1 in the liver represses CTCF binding activity on the ICR, leading to deregulation of the *H19-Igf2* axis, and is associated with increased proliferation. Furthermore, forced expression of *H19* promotes liver cancer cell proliferation by negatively regulating *Phb1*.

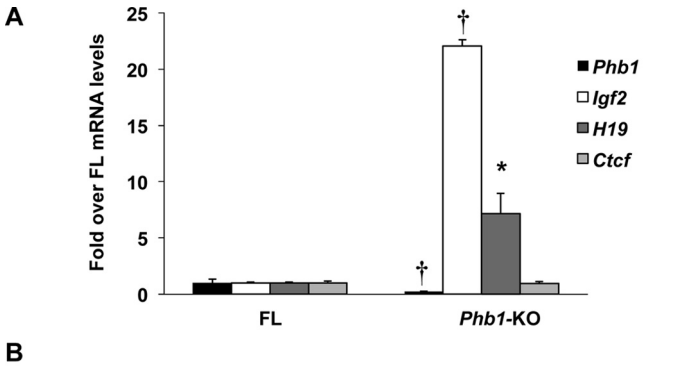

	FL	*Phb1*-KO
PHB1	1±0.04	†0.3±0.06
IGF2	1±0.09	†13.3±1.02
CTCF	1±0.19	0.87±0.11

FIGURE 1. **Induction of *H19* and *Igf2* genes in 3-week-old Phb1 KO mice.** *A*, liver from 3-week-old *Phb1* KO mice and age- and gender-matched floxed (FL) controls was subjected to RNA isolation and real-time RT-PCR as described under "Experimental Procedures." The relative expression of *Phb1*, *Igf2*, *H19*, and *CTCF* in *Phb1* KO livers was compared with FL. Results represent mean ± S.E. from four mice, *, $p < 0.005$, †, $p < 0.001$ *versus* FL. *B*, protein extracted from KO or FL livers was immunoblotted with PHB1, IGF2, CTCF, and actin control antibodies. Representative images and densitometric analysis (mean ± S.E.) from 3–5 mice are shown. †, $p < 0.001$ *versus* FL.

Results

Induction of H19 and Igf2 Genes in 3-week-old Phb1 KO Mice—Three-week-old liver-specific *Phb1*KO mice exhibited ~80% reduction in *Phb*1 mRNA and ~70% reduction in PHB1 protein levels when compared with age-matched control floxed littermates (Fig. 1, *A* and *B*). A 7-fold induction of *H19* mRNA level was observed in KO mice livers when compared with control mice (Fig. 1*A*). *Phb1* KO mice also exhibited a 22-fold induction of *Igf2* mRNA levels (Fig. 1*A*) and a 13-fold induction of IGF2 protein levels when compared with floxed controls (Fig. 1*B*). No change in *Ctcf* mRNA or CTCF protein levels was observed in these mice (Fig. 1, see original blots in supplemental Fig. 1, *A*–*C*). No gender bias was observed with respect to expression of *H19*, *Igf2*, or *Ctcf* in *Phb1* KO mice (data not shown).

In Vitro Silencing of Phb1 in AML12 Cells and Human Liver Cancer Cells Induces H19 and Igf2 Expression—Silencing of *Phb1* by 70–80% in AML12 cells caused a 2-fold induction of *H19* mRNA levels (Fig. 2*A*) and a 2-fold increase in IGF2 mRNA and protein levels (Fig. 2, *A* and *B*) when compared with a negative control siRNA. *Ctcf* mRNA levels remained unchanged (Fig. 2*A*), whereas CTCF protein levels decreased by 30% when compared with negative control (Fig. 2*B*, original blots in supplemental Fig. 2, *A*–*C*). Similar findings were observed in human HCC cell lines (HepG2 and Huh7) after *PHB1* silencing (supplemental Fig. 5, *A* and *B*).

Forced Expression of Ctcf Prevents Phb1 Knockdown-mediated H19 and Igf2 Induction—*Ctcf* mRNA overexpression in AML12 cells treated with negative control or *Phb1* siRNA was 20-fold elevated when compared with empty vector (Fig. 3*A*). CTCF protein levels increased by 2–3-fold when compared with empty vector (Fig. 3*B*). *Phb1* expression was silenced by 65–70% at both the mRNA and the protein levels (Fig. 3, *A* and *B*). *Ctcf* overexpression did not affect endogenous *Phb1* mRNA or PHB1 protein levels in AML12 cells (Fig. 3, *A* and *B*, original blots in supplemental Fig. 3, *A* and *B*). *Ctcf* overexpression inhibited basal *H19* and *Igf2* mRNA levels by 20–30% when compared with empty vector control (Fig. 3*C*). Silencing of *Phb1* enhanced *H19* and *Igf2* expression in empty vector-treated cells (Fig. 3*C*). Forced expression of *Ctcf* in *Phb1* knockdown cells suppressed the induction of *H19* to levels comparable with *Ctcf* overexpression alone and partly suppressed *Igf2* levels when compared with *Phb1* knockdown alone (Fig. 3*C*).

Silencing Ctcf or Phb1 Alone or in Combination Induces H19 and Igf2 Expression—*Ctcf* or *Phb1* silencing (80–90% knockdown, Fig. 4*A*) induced *H19* and *Igf2* mRNA levels by 2-fold when compared with negative control siRNA (Fig. 4*B*). Co-silencing *Ctcf* and *Phb1* did not have an additive effect on *H19*

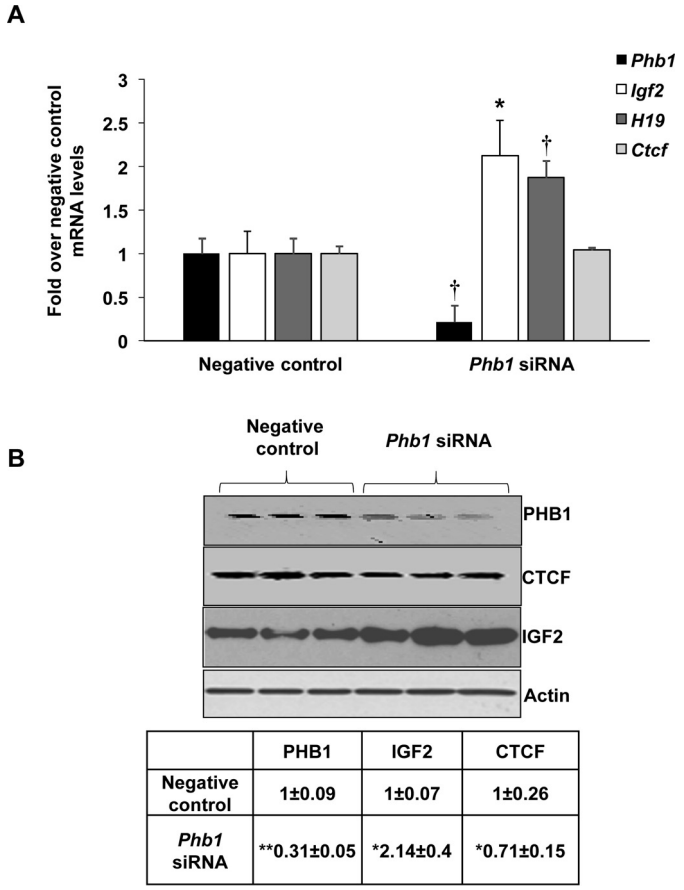

	PHB1	IGF2	CTCF
Negative control	1±0.09	1±0.07	1±0.26
Phb1 siRNA	**0.31±0.05	*2.14±0.4	*0.71±0.15

FIGURE 2. ***In vitro* silencing of *Phb1* in AML12 cells induces *H19* and *Igf2* expression.** AML12 cells were transfected with a negative control or *Phb1* siRNA as described under "Experimental Procedures." *A* and *B*, cells were processed for real-time RT-PCR for *Phb1*, *Igf2*, *H19*, and *Ctcf* mRNA (*A*) or Western blotting and densitometric analysis for PHB1, IGF2, and CTCF proteins (*B*). Results represent mean ± S.E. of 3–4 experiments. *, $p < 0.05$, **, $p < 0.005$, †, $p < 0.001$ *versus* negative control.

and *Igf2* induction, suggesting that CTCF and PHB1 operate in concert to repress the *H19-Igf2* axis (Fig. 4*B*).

CTCF and PHB1 Interact and Co-localize on the ICR Element Controlling H19 and Igf2 Genes in AML12 Cells—*H19* and *Igf2* genes are located on a well characterized imprinted gene cluster that is controlled by an ICR in the 5′-flank of the *H19* gene and by a shared enhancer downstream of *H19* (20). As shown in Fig. 5*A*, the ICR contains four CTCF-binding sites. The two CTCF-binding sites in ICR region 1 are 2814 bp upstream of the *H19* promoter, whereas those in ICR region 2 are 1414 bp upstream of the *H19* promoter. ICR regions 1 and 2 were amplified after ChIP and sequential ChIP to examine the localization of CTCF and PHB1 on these regions. Both ICR region 1 and ICR region 2 exhibited immunoprecipitation with CTCF antibody (Fig. 5*B*, *left panel*). Quantitative PCR estimation of the target site occupancy of CTCF on these regions demonstrated that CTCF binding to region 1 was 4-fold higher than that of region 2 (Fig. 5*B*, *right panel*). ICR region 1, but not region 2, exhibited detectable immunoprecipitation with the PHB1 antibody alone (Fig. 5*B*). However, sequential immunoprecipitation of the ICR sites with CTCF followed by PHB1 antibody (sequential ChIP, CTCF:PHB1) demonstrated that PHB1 co-localized with CTCF at these sites (Fig. 5*B*). CTCF co-immunoprecipitated with endogenous PHB1 and vice versa in AML12 extracts and also with overexpressed PHB1 in these cells (PHB1-DDK) (Fig. 5*C*, original blots in Supplemental Fig. 4, *A* and *B*). These results suggest that PHB1 and CTCF interact with each other and that PHB1 localizes on the ICR by virtue of its interaction with CTCF.

In Vitro Silencing of Phb1 in AML12 Cells Inhibits the Binding of CTCF to the ICR That Is Partly Recovered by Ctcf Overexpression—We performed ChIP analysis to examine whether PHB1 was required for CTCF binding to the ICR. *Phb1* siRNA transfection in AML12 cells lowered the binding of CTCF to ICR regions 1 and 2 by 80% when compared with a negative control siRNA (Fig. 6*A*), suggesting that PHB1 is required to maintain the binding of CTCF to these regions. *Ctcf* overexpression induced CTCF binding to the ICR (Fig. 6*A*). When compared with *Phb1* silencing alone, AML12 cells co-expressing *Ctcf* vector and *Phb1* siRNA exhibited partial recovery of CTCF binding to ICR region 1 and complete recovery of CTCF binding to region 2 (Fig. 6*A*). ChIP analysis was further confirmed by performing EMSA with supershift of a synthetic CTCF-binding site fragment containing the four CTCF-binding sites of the ICR (see "Experimental Procedures"). Nuclear extracts from *Ctcf*-overexpressing AML12 cells exhibited increased binding and supershift with CTCF antibody (Fig. 6*B*). *Phb1* knockdown extracts exhibited lower CTCF binding and supershift when compared with control. *Ctcf* overexpression partially recovered the binding of CTCF in *Phb1* knockdown cells when compared with both negative control and *Phb1* silencing alone (Fig. 6*B*).

CTCF and PHB1 Interact and Co-localize on the ICR Regulatory Element Controlling H19 and Igf2 Genes in Normal Mouse Liver—We next examined the co-occupancy of CTCF and PHB1 to ICR in mouse liver to make sure that the findings in AML12 cells were also true in liver. Both ICR region 1 and ICR region 2 from mouse liver chromatin immunoprecipitated with CTCF antibody (Fig. 7*A*, *top panel*). The amplification of ICR region 1 was very similar between the four livers tested, whereas it was variable in ICR region 2 (Fig. 7*A*). ICR regions 1 and 2 showed very low immunoprecipitation with PHB1 antibody (Fig. 7*A*). Consistent with the *in vitro* findings in Fig. 5, sequential ChIP also detected PHB1 in CTCF-immunoprecipitated chromatin (Fig. 7*A*, both ICR region 1 and ICR region 2). Co-immunoprecipitation analysis of total liver with PHB1 antibody showed that CTCF and PHB1 interacted with each other *in vivo* (Fig. 7*B*), confirming the *in vitro* results from Fig. 5*C*.

CTCF Binding to the ICR Is Reduced in Phb1 KO Mouse Liver—An *in vivo* ChIP assay was designed to evaluate the binding of CTCF to ICR in mouse liver chromatin from *Phb1* KO and floxed control mice. Our results showed that the immunoprecipitation of the ICR regions by CTCF antibody was suppressed in *Phb1* KO mice when compared with floxed controls (Fig. 8, *top panel*). However, because agarose gel data on CTCF to ICR binding were very qualitative and there appeared to be variability in the extent of inhibition between different livers, we quantified the exact target site occupancy of CTCF to the ICR by real-time PCR. Our results showed that CTCF occupancy was reduced by 60% in *Phb1* KO mice when compared with floxed controls (Fig. 8, *bottom panel*).

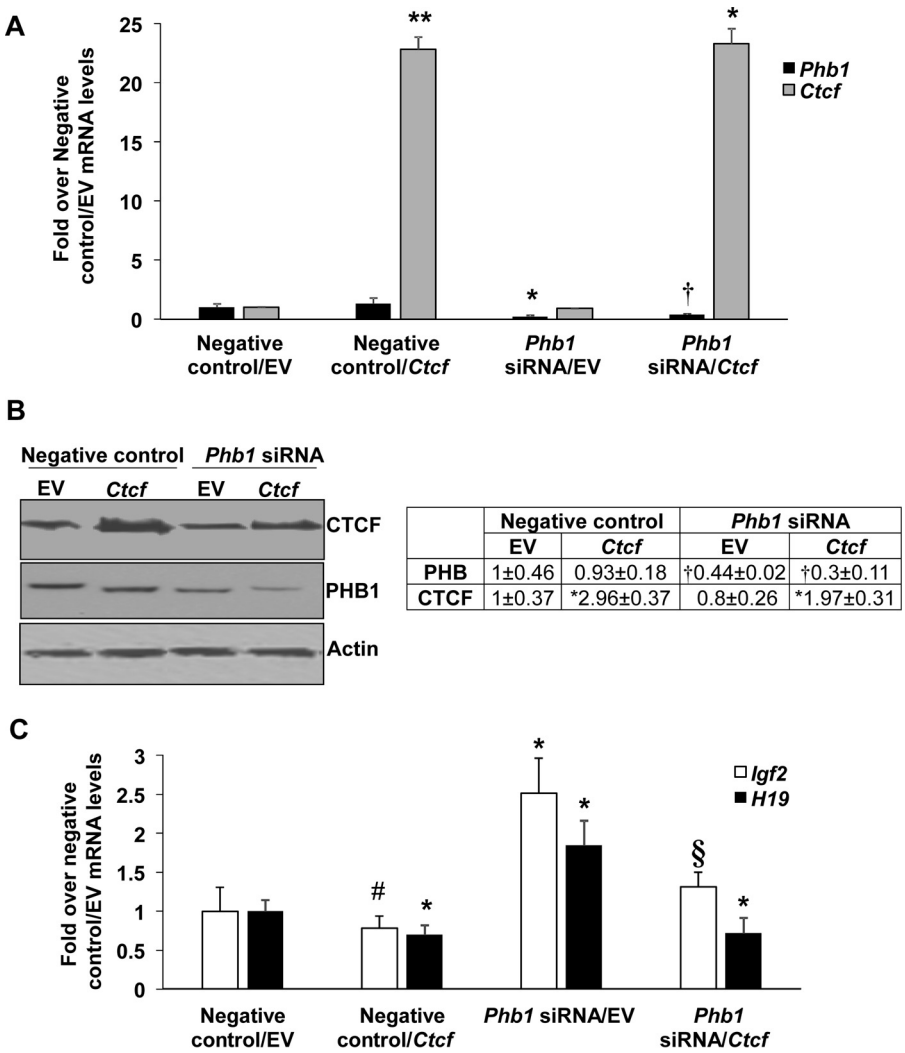

	Negative control		*Phb1* siRNA	
	EV	*Ctcf*	EV	*Ctcf*
PHB	1±0.46	0.93±0.18	†0.44±0.02	†0.3±0.11
CTCF	1±0.37	*2.96±0.37	0.8±0.26	*1.97±0.31

FIGURE 3. **Forced expression of Ctcf prevents *Phb1* knockdown-mediated *H19* and *Igf2* induction.** AML12 cells were transfected with *Phb1* siRNA, *Ctcf* expression vector, or both as described under "Experimental Procedures." Negative control siRNA, empty vector (EV), or both were used as transfection controls. *A* and *B*, the efficiency of silencing or overexpression was measured by real-time RT-PCR for *Phb1* and *Ctcf* mRNA (*A*) or Western blotting and densitometric analysis for PHB1 and CTCF proteins (*B*). *C*, the effect of knockdown or overexpression on *H19* and *Igf2* mRNA expression was assessed by real-time RT-PCR. Results represent mean ± S.E. of 4 experiments. *, $p < 0.05$, **, $p < 0.005$, #, $p < 0.01$, †, $p < 0.001$ *versus* negative control/EV, §, $p < 0.05$ *versus* negative control/*Ctcf*.

Expression of IGF2 and H19 Negatively Correlates with PHB1 and CTCF Expression and ICR Binding in Human HCC—Next, we analyzed human HCC and normal liver tissues for the expression levels of *PHB1*, *CTCF*, *H19*, and *IGF2*. A significant 40–50% reduction in the mRNA expression levels of *PHB1* and *CTCF* and a 40–50-fold increase in *H19* and *IGF2* were observed in HCC tissues when compared with normal liver tissues (Fig. 9*A*). Importantly, ICR target occupancy of CTCF and PHB1 was significantly reduced in HCC when compared with normal liver tissues (Fig. 9*B*).

Modulation of H19 Gene Influences Phb1-mediated Cellular Proliferation in Liver Cancer Cells—So far our results have demonstrated that the *H19* and *Igf2* genes are induced during *Phb1* depletion. PHB1 controls the *H19-Igf2* axis by interacting and co-localizing with CTCF on the ICR regulatory region controlling both genes. Our previously published work showed that *Phb1* KO mice develop HCC (12). To examine whether *Phb1* modulation could lead to tumorigenesis in part via *H19*, we examined the effect of silencing or overexpressing *Phb1* or *H19* on proliferation of the liver cancer cell line, *S*-adenosylmethionine-deficient (SAMe-D), which is derived from the methionine adenosyltransferase 1a KO (*Mat1a* KO) mouse model of HCC (21). The expression of *Phb1* in SAMe-D cells was lower than AML12 hepatocytes (data not shown). Transfection of *Phb1* or *H19* siRNA in SAMe-D cells caused a 90% knockdown of *Phb1* and *H19* mRNA levels, respectively (Fig. 10*A*, *left panel*). Silencing *Phb1* induced endogenous *H19* mRNA levels, and *H19* silencing induced both endogenous *Phb1* mRNA and endogenous PHB1 protein levels (Fig. 10*A*, *left* and *right panels*), indicating a reciprocal regulation between PHB1 and *H19*. We further examined whether the cross-regulation between PHB1 and *H19* could alter cell growth. SAMe-D cells were transfected with *Phb1*, *H19*, or both siRNAs. Silencing *Phb1* induced the growth of SAMe-D cells by 1.6-fold when compared with a negative control (Fig. 10*B*). Silencing *H19* caused a 25% decrease in cell growth when compared with negative control (Fig. 10*B*). Co-silencing of *H19* with *Phb1* inhibited the inductive effect of *Phb1* silencing on SAMe-D proliferation

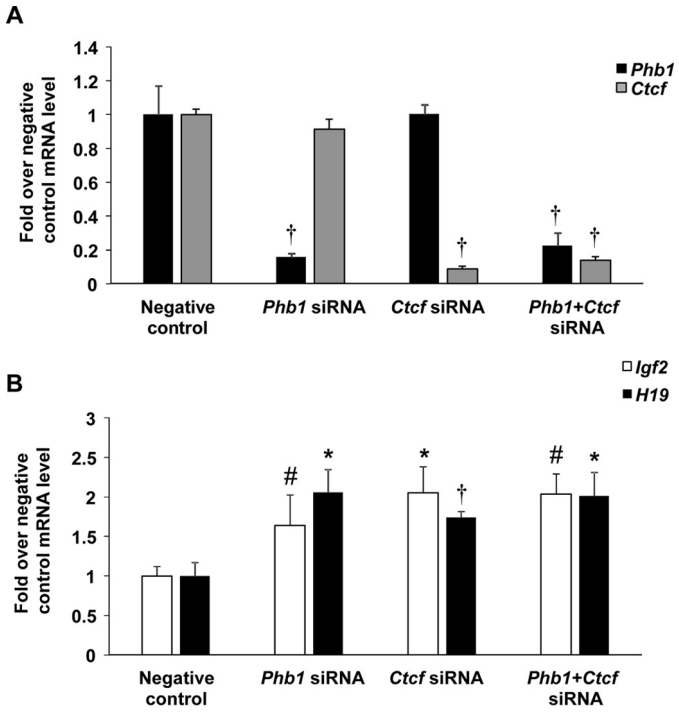

FIGURE 4. **Silencing *Ctcf* or *Phb1* alone or in combination induces *H19* and *Igf2* expression.** AML12 cells were transfected with *Phb1* siRNA, *Ctcf* siRNA, or both as described under "Experimental Procedures." Negative control siRNA was used as a transfection control. *A*, the efficiency of silencing was measured by real-time RT-PCR for *Phb1* and *Ctcf* mRNA. *B*, the effect of silencing on *H19* and *Igf2* mRNA expression was assessed by real-time RT-PCR. Results represent mean ± S.E. of 3 experiments. *, $p < 0.05$, #, $p < 0.01$, †, $p < 0.001$ *versus* negative control siRNA.

(Fig. 10*B*). The silencing data on cell proliferation were confirmed by overexpressing *Phb1*, *H19*, or both in SAMe-D cells. *Phb1* or *H19* overexpression in SAMe-D cells induced these genes by 34- and 16-fold, respectively, when compared with empty vector (relative *Phb1* mRNA expression: empty vector = 1 ± 0.27, *Phb1* vector = *34.35 ± 5.9; relative *H19* mRNA expression: empty vector = 1 ± 0.39, *H19* vector = †16.25 ± 3.76, *, $p < 0.05$, †, $p < 0.001$ *versus* empty vector). Overexpressing *Phb1* suppressed endogenous *H19* mRNA levels when compared with empty vector (relative *H19* mRNA expression: empty vector = 1 ± 0.39, *Phb1* vector = †0.68 ± 0.02, †, $p <$ 0.001 *versus* empty vector), and *H19* overexpression suppressed endogenous *Phb1* mRNA levels (relative *H19* mRNA expression: empty vector = 1 ± 0.27, *Phb1* vector = *0.51 ± 0.16, *, $p < 0.05$ *versus* empty vector). *Phb1* overexpression inhibited SAMe-D growth by 30% when compared with an empty vector control (Fig. 10*C*). *H19* overexpression caused a 1.6-fold induction in cell growth when compared with empty vector (Fig. 10*C*). Forced co-expression of *H19* with *Phb1* reversed the suppressive effect of PHB1 on growth (Fig. 10*C*), thereby confirming a reciprocal regulation between *Phb1* and *H19* in SAMe-D cells. The results suggest that the suppressive effect of *Phb1* on cell growth may be mediated at least in part by its inhibition of *H19* expression, and because silencing *H19* induced *Phb1* (Fig. 10*A*), this could also inhibit cell growth (Fig. 9*B*). Low expression of *H19* is associated with high PHB1 level that suppresses cell growth, whereas high expression of *H19* is associated with lower PHB1 level that enhances cell growth. These results strongly support the role of *H19* gene deregulation in preventing the tumor suppressor activity of *Phb1* in liver cancer cells.

Discussion

The tumor modulatory activity of PHB1 is cell type-specific and likely depends on its subcellular localization and post-translational modifications. A strong correlation exists between *Phb1* deficiency and conditions leading to rapid liver growth such as following partial hepatectomy, or increased propensity to HCC such as nonalcoholic steatohepatitis and ethanol abuse (11, 22). Despite these findings, the mechanism of action of PHB1 as a cell proliferation control point in the liver is not clearly established. Although liver-specific *Phb1* KO mice develop HCC spontaneously, this may have occurred due to the severe liver injury and regenerative response (12). Nevertheless, we observed an inverse relationship between PHB1 expression and growth in the nonmalignant AML12 hepatocyte cell line, suggesting that PHB1 plays a direct growth modulatory role (12). Part of this mechanism may be related to the suppressive effect of PHB1 on E2F *trans*-activating activity (9). Consistent with this, E2F binding to the cyclin D1 promoter and cyclin D1 expression were higher in liver-specific *Phb1* KO livers (12). However, two tumor growth-associated genes, *H19* and *Igf2*, are also induced in *Phb1* KO livers of young 3-week-old mice in both genders (12), which prompted us to hypothesize that *Phb1* is involved in regulating the *H19-Igf2* axis in normal liver and that this may be another important mechanism controlling liver cell proliferation. In the course of this work, we uncovered a previously unrecognized role of PHB1 in modulating the activity of CTCF as well as the reciprocal regulation between PHB1 and *H19*.

We probed the factors that were known to regulate the *H19-Igf2* gene cluster. One such critical factor, CTCF, negatively regulates the ICR by direct binding, and this CTCF-ICR interaction blocks *Igf2* expression on the maternal allele (23). On the other hand, the paternal allele is methylated, and thus CTCF-ICR interaction is prevented, thereby allowing *Igf2* to be expressed. *H19* expression is regulated by methylation of the ICR (13, 24). Methylation on the paternal allele blocks *H19* expression. Hence it is only maternally expressed (13, 24). Deletion of the ICR results in biallelic expression of both *Igf2* and *H19* (20). A direct effect of CTCF on *H19* has not been reported so far. Because CTCF-ICR interaction is a major player in regulating the *H19-Igf2* axis and there was deregulation of this axis upon *Phb1* depletion, we hypothesized that the CTCF-ICR interaction may be modulated by PHB1 to control this axis in normal cells. To evaluate this hypothesis, we examined whether *Phb1* silencing affected *Ctcf* expression. *Phb1* KO mice did not exhibit any change in *Ctcf* mRNA or protein levels. However, *in vitro* silencing of *Phb1* in normal AML12 hepatocytes did not affect *Ctcf* mRNA levels but moderately lowered CTCF protein levels. The difference between the *in vitro* silencing and *in vivo* deletion may be due to compensatory effects that prevented down-regulation of CTCF expression *in vivo*. Nevertheless, *Phb1* silencing did not alter *Ctcf* expression dramatically and hence could not be responsible for the increase in *H19* and *Igf2* expression observed *in vitro* and *in vivo*. However, because it is known that CTCF is a regulator of the ICR that controls the

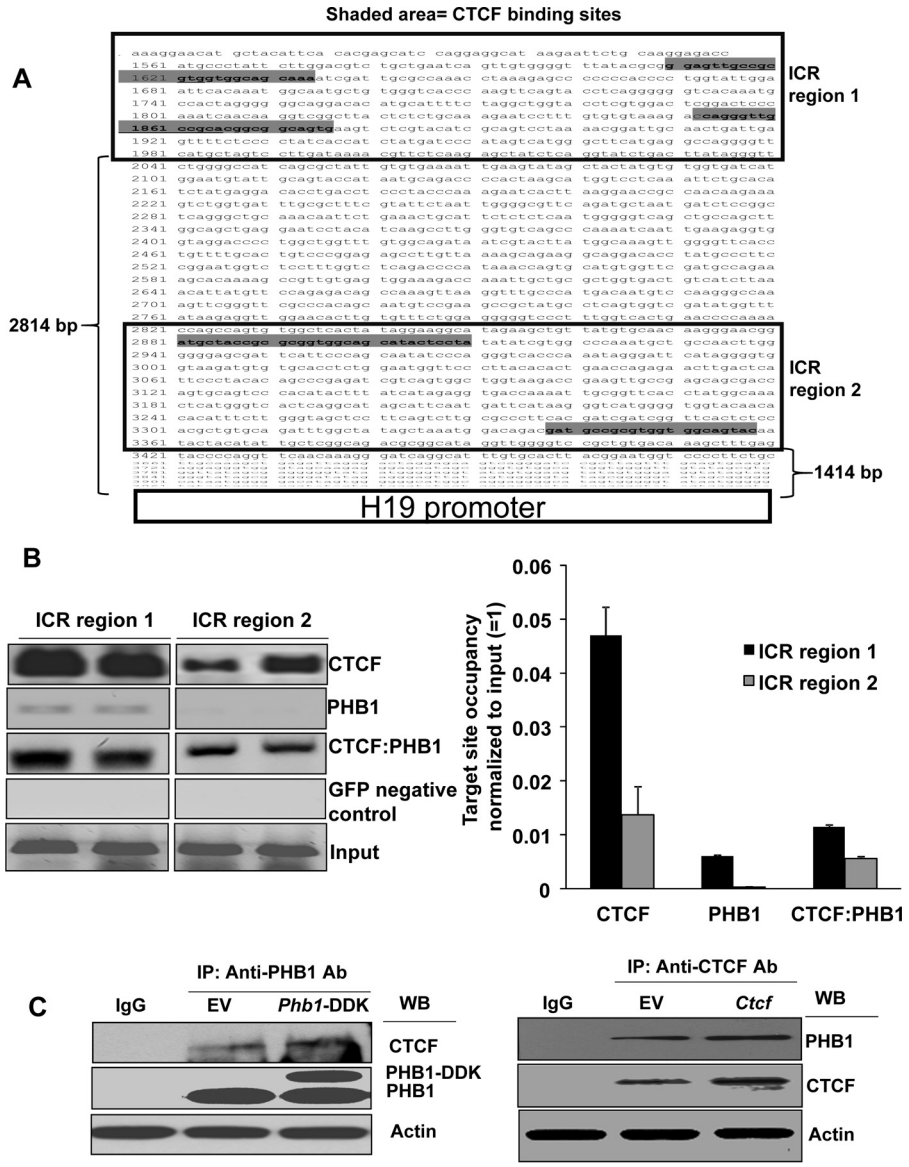

FIGURE 5. **CTCF and PHB1 interact and co-localize on the ICR element controlling *H19* and *Igf2* genes in AML12 cells.** *A*, the position and sequence of the four CTCF-binding sites relative to the *H19* promoter (accession ID: AF049091.1). *B*, the co-localization of CTCF and PHB1 on the ICR region 1 (343-bp amplicon) and region 2 (552-bp amplicon) was assessed by sequential ChIP of chromatin from AML12 cells as described under "Experimental Procedures." The *left panel* is a representative agarose gel of the PCR products, and the *right panel* is the real-time PCR quantification of the target site occupancy of CTCF and PHB1 on the ICR regions. GFP antibody was used as a ChIP control. Results represent mean ± S.E. from 3 experiments in duplicates. *C*, endogenous PHB1 protein or overexpressed PHB1 (PHB1-DDK) from AML12 extracts was immunoprecipitated (*IP*) with PHB1 antibody (*Ab*) and immunoblotted (*WB*) for CTCF detection (*left panel*). The same blot was re-probed with PHB1 antibody. Endogenous CTCF or overexpressed CTCF was immunoprecipitated with CTCF antibody and immunoblotted for PHB1 detection. The same blot was re-probed with CTCF antibody (*right panel*). Actin was used as a loading control. A representative immunoblot from 2 independent experiments is shown.

H19-Igf2 axis, we examined whether PHB1 could regulate CTCF-ICR interaction to affect the expression of these genes. *Ctcf* overexpression in AML12 cells caused a 20–30% suppression of basal *H19* and *Igf2* mRNA levels, whereas *Ctcf* silencing induced *H19* and *Igf2* by 2-fold. *Ctcf* overexpression suppressed induction of *H19* and *Igf2* caused by *Phb1* silencing, indicating that PHB1 and CTCF cooperated with each other to regulate *H19* and *Igf2* expression. *Ctcf* or *Phb1* depletion in AML12 induced both *H19* and *Igf2* levels. Co-silencing of *Phb1* and *Ctcf* did not have an additive effect on *H19* and *Igf2*, further supporting the notion that PHB1 and CTCF act in concert to regulate the *H19-Igf2* axis.

To examine how the PHB1-CTCF partnership might affect *H19* and *Igf2* in the liver, we examined interactions of PHB1 and CTCF with the ICR element and with each other both *in vitro* and *in vivo*. Sequential ChIP and EMSA analysis demonstrated that PHB1 co-localized with CTCF on the CTCF-binding regions of the ICR. From co-immunoprecipitation studies, we demonstrated that both CTCF and PHB1 interacted with each other. To examine whether PHB1 was required for CTCF ICR binding activity, we examined CTCF binding to the ICR in *Phb1*-depleted AML12 cells or in *Phb1* KO livers. Our results clearly demonstrate that PHB1 depletion substantially reduces the localization of CTCF on the ICR. These data together pro-

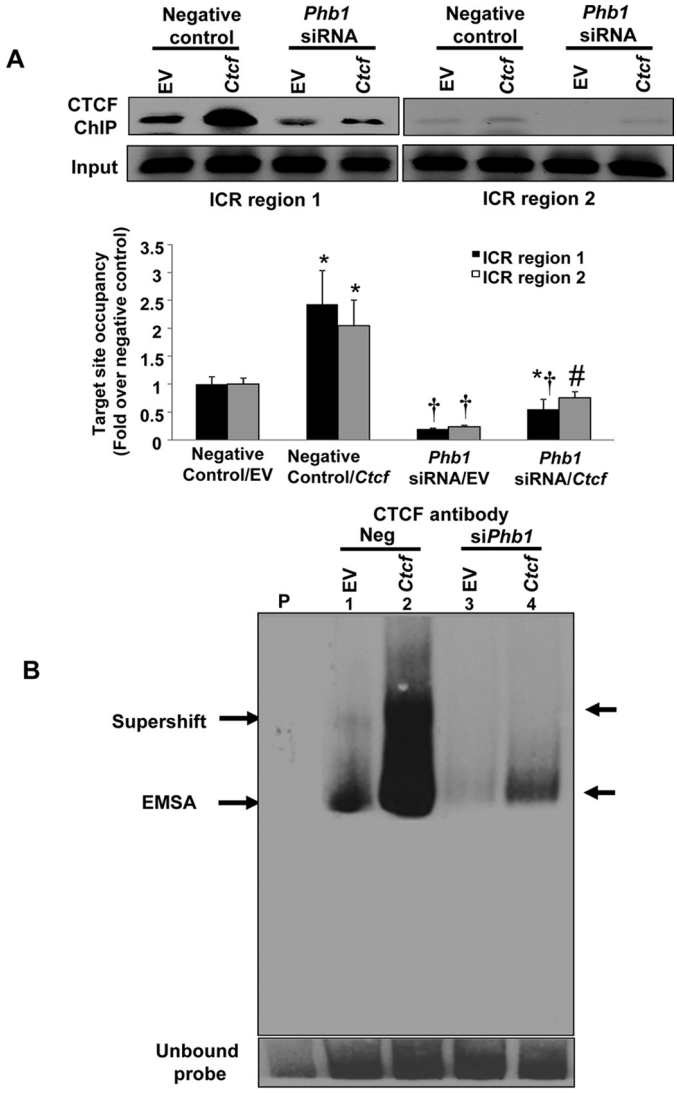

FIGURE 6. ***In vitro* silencing of *Phb1* in AML12 cells inhibits the binding of CTCF to the ICR that is partly recovered by *Ctcf* overexpression.** *A*, AML12 cells were transfected with negative control or *Phb1* siRNA in the presence of either EV or *Ctcf* overexpression, and total chromatin was immunoprecipitated with CTCF antibody as described under "Experimental Procedures." The immunoprecipitated DNA was amplified by PCR to detect CTCF binding on ICR regions 1 and 2 (*top panel*, agarose gel; *bottom panel*, real-time PCR for target site occupancy quantification). Relative target site occupancy represented as -fold over negative control is mean ± S.E. from 3 experiments. *, $p < 0.05$ *versus* negative control siRNA, †, $p < 0.001$ *versus* negative control or *Phb1* siRNA, #, $p < 0.01$ *versus Phb1* siRNA. *B*, AML12 cells were transfected with negative control/empty vector, *Phb1* siRNA, *Ctcf* expression vector, or *Phb1* siRNA+*Ctcf* vector, and EMSA with supershift of nuclear extracts was performed as described under "Experimental Procedures." *Lanes 1–4*: EMSA with supershift of a biotinylated CTCF-binding site probe with CTCF antibody. Key: *p* = probe only, *EV* = empty vector, *Neg* = Negative control siRNA, *siPhb1* = *Phb1* siRNA. A representative blot from three experiments is shown.

vide a novel mechanism of control of the *H19-Igf2* axis by CTCF that requires PHB1. Lack of PHB1 lowers CTCF binding activity on the ICR, thereby deregulating the *H19-Igf2* axis, and this could be a probable mechanism for induction of growth in liver cells. Further evidence of the importance of this regulation comes from human HCC tissues where low *PHB1* and *CTCF* levels and ICR binding activity of the proteins are associated with high levels of *H19* and *IGF2* genes. It is known that the *H19-Igf2* axis is deregulated in HCC tissues and hepatoblastoma cell lines and during hepatocyte proliferation (14, 15, 19). To our knowledge, this is the first study providing mechanistic insight into the control of this axis in normal liver by the unique interaction of PHB1 with CTCF, a known modulator of the ICR region (23).

Our previously published work showed that normal AML12 hepatocytes depleted of *Phb1* exhibit enhanced cellular proliferation (12). Although we showed that both *H19* and *Igf2* genes were deregulated upon *Phb1* silencing, in this work, we focused on *H19-Phb1* interplay as a growth modulatory mechanism because a direct effect of *H19* on liver cancer growth has not been established so far, whereas the molecular aspects of IGF2 signaling inducing HCC growth are well established (17). To understand whether *Phb1* modulation in liver cancer cells had a functional effect on growth and whether this involved *H19* interplay, we silenced *Phb1* in the SAMe-D mouse HCC cell line. Silencing *Phb1* induced proliferation of SAMe-D cells. Co-silencing of *H19* in these cells blunted both basal and *Phb1* depletion-induced cell growth, whereas *H19* overexpression reversed the suppressive effect of PHB1 on growth. Interestingly, *H19* silencing also induced endogenous PHB1 mRNA and protein levels in SAMe-D cells. Our results suggest that elevated *H19* expression in liver cancer cells may promote cell proliferation, in part by suppressing *Phb1* expression. An interesting question arising from these findings is: How does *H19* suppress *Phb1* expression in liver cancer cells? One probable way could be through microRNA regulation. It is well established that *H19* acts as a molecular sponge for various microRNAs that regulate epithelial-to-mesenchymal transition and pathways associated with oncogenic phenotypes (25). *Phb1* is also regulated by microRNAs such as miR-26a and miR-27a in gliomas and gastric cancer (3). However, *H19*-regulated microRNAs that may regulate *Phb1* expression in the liver have not been described so far and would constitute a future area of study.

In summary, we have identified a novel mechanism by which PHB1 and CTCF cooperate with each other to control the expression of *H19* and *Igf2* genes. Loss of this control caused by *Phb1* depletion induces the expression of these genes and favors hepatocyte proliferation. Induction of *H19*, in turn, reverses the growth-suppressive effect of PHB1, in part by reducing PHB1 expression in liver cancer cells.

Experimental Procedures

Materials—All buffers and chemicals were purchased from Sigma and were of molecular biology grade.

Human Liver Tissue Collection—Human liver tissues were collected by following Institutional Review Board (IRB) protocols approved by the Cedars-Sinai Medical Center and University of Southern California Keck School of Medicine. Written informed consent was obtained from each patient. Normal liver tissue was obtained from five patients with metastatic colon or breast carcinoma. Cancerous liver tissue was obtained from 11 patients undergoing surgical resection for primary HCC. The contamination of HCC samples with noncancerous tissue was less than 5% as determined by histopathology. These tissues were immediately frozen in liquid nitrogen for subsequent experiments.

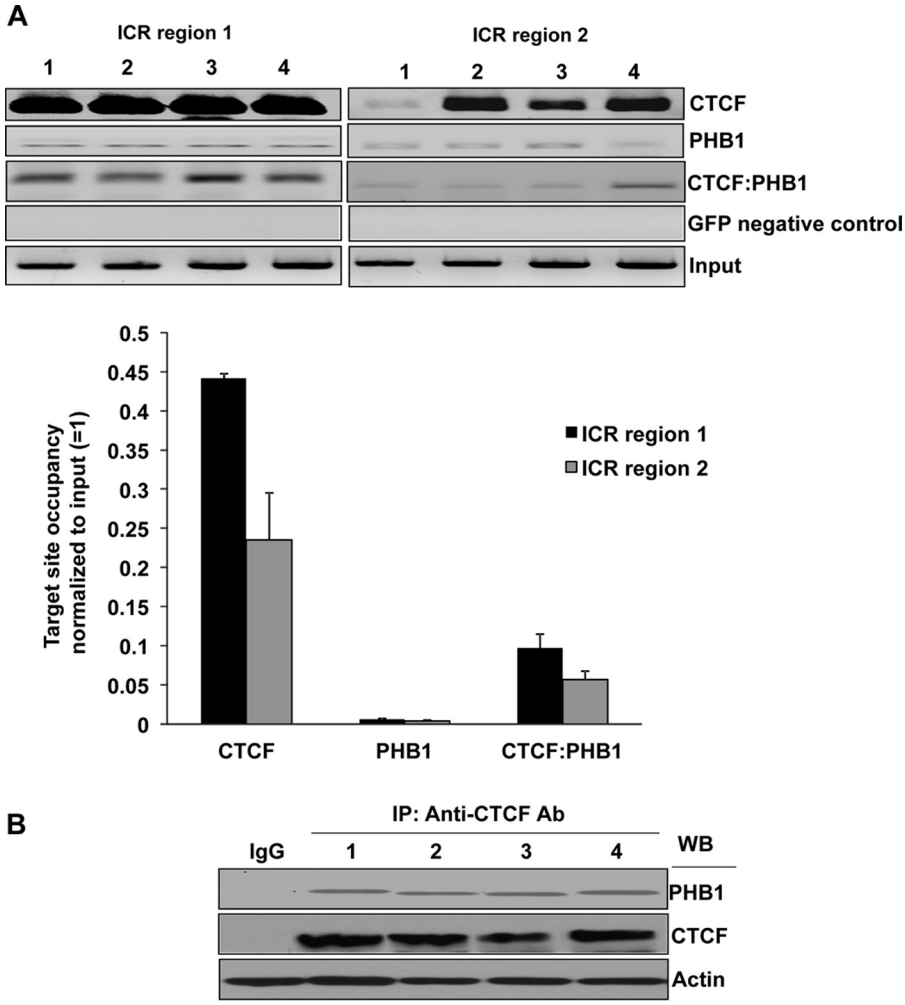

FIGURE 7. **CTCF and PHB1 interact and co-localize on the ICR regulatory element controlling *H19* and *Igf2* genes in normal mouse liver.** *A*, the co-localization of CTCF and PHB1 on the ICR region 1 (343-bp amplicon) and region 2 (552-bp amplicon) was assessed by sequential ChIP of total liver chromatin as described under "Experimental Procedures." The PCR products were electrophoresed on a 1% agarose gel (*top panel*). GFP antibody was used as a ChIP control. The target site occupancy of CTCF and PHB1 on the ICR regions was measured by real-time PCR (*bottom panel*). Results represent mean ± S.E. from four normal mouse livers. *B*, endogenous PHB1 protein from total liver extracts was immunoprecipitated (*IP*) with CTCF antibody (*Ab*) using normal IgG as a control and immunoblotted (*WB*) for PHB1 detection. The same blot was re-probed with CTCF antibody. Actin was used as a loading control. Results from four mouse livers are shown.

Animals—Three-week-old liver-specific *Phb1* KO mice and corresponding floxed control mice have been described previously (12). Livers from these mice were processed for experiments as described below. All animal procedures were performed by established protocols approved by the Institutional Animal Care and Use Committee (IACUC) of the Cedars-Sinai Medical Center, which has been American Association of Laboratory Animal Care (AAALAC)-accredited since 1967. Animals were treated humanely, and all procedures were in compliance with the institution's guidelines for the use of laboratory animals.

Cell Culture and Transfections—The AML12 normal mouse hepatocyte cell line was purchased from American Type Culture Collection (ATCC: CRL2254) and cultured in DMEM-F12 medium containing 10% serum, 0.005 mg/ml insulin, 0.005 mg/ml transferrin, 5 ng/ml selenium, and 40 ng/ml dexamethasone. SAMe-D cells are derived from HCC obtained from *Mat1a* KO mouse and were cultured in DMEM supplemented with 10% FBS and 100 units/ml penicillin, 0.1 mg/ml streptomycin, and 2 mmol/liter L-glutamine (21). HepG2 and Huh7 cells were cultured in DMEM supplemented with 10% FBS and 100 units/ml penicillin, 0.1 mg/ml streptomycin, and 2 mmol/liter L-glutamine. Pre-validated Silencer® Select siRNAs against *Phb1*, *Igf2*, and *H19* siRNAs were purchased from Thermo Fisher Scientific. The siRNAs were reverse-transfected into cells at a dose of 20 nM in 6-well plates or 96-well plates using the Lipofectamine RNAiMAX™ transfection reagent (Invitrogen) for 24–72 h. Expression plasmids for *Phb1* (encoding for PHB1-DDK tagged protein), *H19*, and *CTCF* were purchased from OriGene (Rockville, MD) and forward-transfected at a concentration of 0.5 μg/ml in 6-well plates or 96-well plates using the jetPRIME® reagent (Polyplus-transfection, Radnor, PA) according to the manufacturer's protocol.

RNA Isolation, Reverse Transcription, and Real-time RT-PCR—For cultured cells, DNA-free RNA was isolated using a column-based purification method according to the manufacturer's protocol (Quick-RNA™ MiniPrep, Zymo Research, Irvine, CA). For mouse tissues, RNA was first extracted from tissue

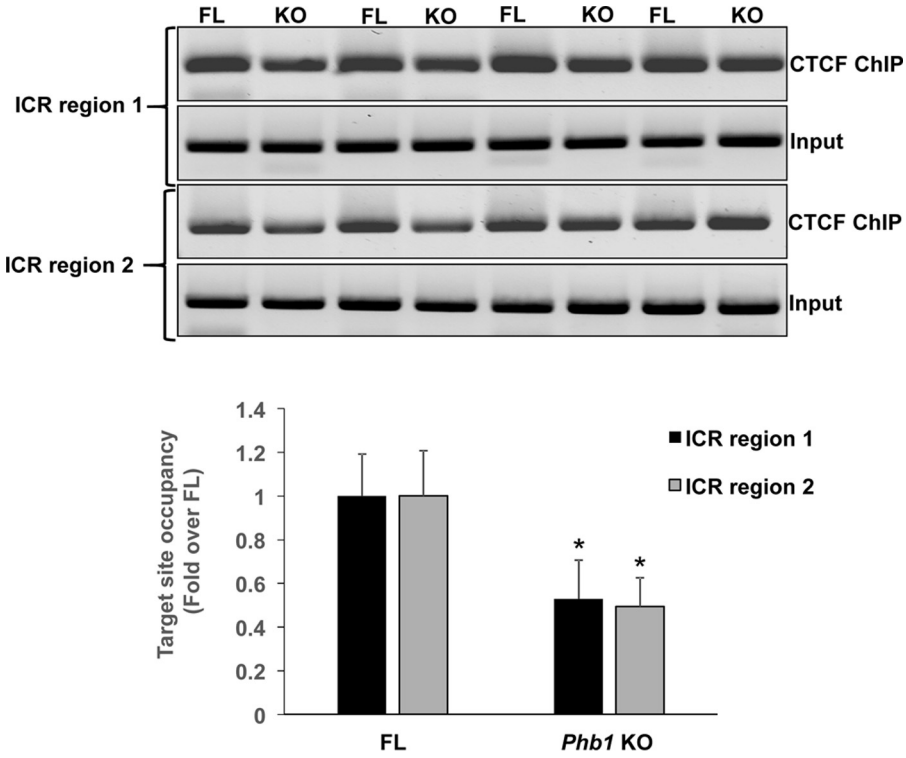

FIGURE 8. **CTCF binding to the ICR is reduced in *Phb1* KO mouse liver.** Chromatin from FL or *Phb1* KO mice was immunoprecipitated with CTCF antibody as described under "Experimental Procedures." The immunoprecipitated DNA was amplified by PCR to detect CTCF binding on ICR regions 1 and 2 (*top panel*). Target site occupancy of CTCF was quantified by real-time PCR (*bottom panel*). The relative target site occupancy represented as -fold over negative control is mean ± S.E. from 4 mice. *, $p < 0.05$ *versus* FL.

homogenized using the TRIzol® reagent (Invitrogen), and then phenol-extracted supernatants were loaded onto Quick-RNA™ MiniPrep (Zymo Research) to obtain DNA-free RNA. One microgram of total RNA from cells or tissues was reverse-transcribed using 100 units of NxGen® M-MuLV Reverse Transcriptase according to the manufacturer's protocol (Lucigen Corp., Middleton, WI). Quantitative real-time PCR was performed using TaqMan® or SYBR® Green-based primer/probes. TaqMan® probes for *Phb1*, *CTCF*, and *H19*, and control gene *GAPDH*, were purchased from Applied Biosystems (Foster City, CA). SYBR® Green cDNA-specific primers for *Igf2* were: forward, 5′-CTTCAGTTTGTCTGTTCGGACCG-3′; reverse, 5′-TGGCACAGTATGTCT-3′. For TaqMan®-based real-time PCR, the thermal profile consisted of initial denaturation at 95 °C for 15 min followed by 45 cycles at 95 °C for 15 s and at 60 °C for 1 min. For SYBR® Green-based real-time PCR, the thermal profile consisted of an initial denaturation at 95 °C for 3 min, PCR of 45 cycles at 95 °C for 30 s, 54 °C for 30 s, 72 °C for 1 min, and a final extension at 72 °C for 10 min. Melting curve analysis was as follows: 95 °C for 5 min, 65 °C for 1 min, and 97 °C for 30 min. Relative mRNA levels were calculated from the cycle threshold (Ct value) of target genes normalized to that of GAPDH to obtain the ΔCt. The ΔCt was used to find the relative expression of target genes according to the formula: relative expression $= 2^{-\Delta\Delta Ct}$, where ΔΔCt = ΔCt of target genes in experimental condition − ΔCt of target gene under control condition.

Western Blotting and Co-immunoprecipitation Assays—Total cellular protein from AML12 cells, SAMe-D cells, or liver tissue prepared using radioimmunoprecipitation assay buffer containing protease inhibitor cocktail (Sigma) was subjected to SDS-PAGE followed by Western blotting according to standard methods (Amersham Biosciences). Antibodies used for Western blotting were: PHB1 and IGF2 (Abcam, Cambridge, MA), CTCF (Cell Signaling, Danvers, MA), and actin control (Sigma). For co-immunoprecipitation, 500 μg of radioimmunoprecipitation assay extracts of cells or tissues were immunoprecipitated with 2 μg of PHB1 antibody and immunoblotted with CTCF antibody according to previously established protocols (26). Western blots were developed using the chemiluminescence ECL system (Amersham Biosciences). Blots were quantified using the ImageJ densitometry program (National Institutes of Health), and test protein expression was normalized to actin control.

ChIP, Sequential ChIP, and SYBR® Green Real-time PCR—The localization of CTCF and PHB1 on the CTCF-binding sites of the ICR was examined by ChIP assay using the EpiTect® ChIP OneDay protocol (Qiagen, Valencia, CA). This kit was also used for sequential ChIP to study the co-localization of CTCF and PHB1 on the ICR. Briefly, chromatin immunoprecipitated by CTCF antibody was processed for a second round of immunoprecipitation using PHB1 antibody. The final, purified DNA was detected by PCR analysis. Antibodies used for ChIP were the same as those used in Western blotting. GFP antibody was used as a negative control for ChIP. The ICR region 1 (343 bp) and region 2 (552 bp) upstream of the *H19* promoter (accession ID: AF049091.1, Fig. 5*A*) containing two CTCF-binding sites each were amplified with the following PCR primers: ICR1-forward, 5′-GGACGTCTGCTGAATCAGTTGT-3′; ICR1-reverse, 5′-TCAGTTGCAATCCGTTTTAGG-3′; ICR2-forward, 5′-GGCTCACTATAGGAAGGCA-

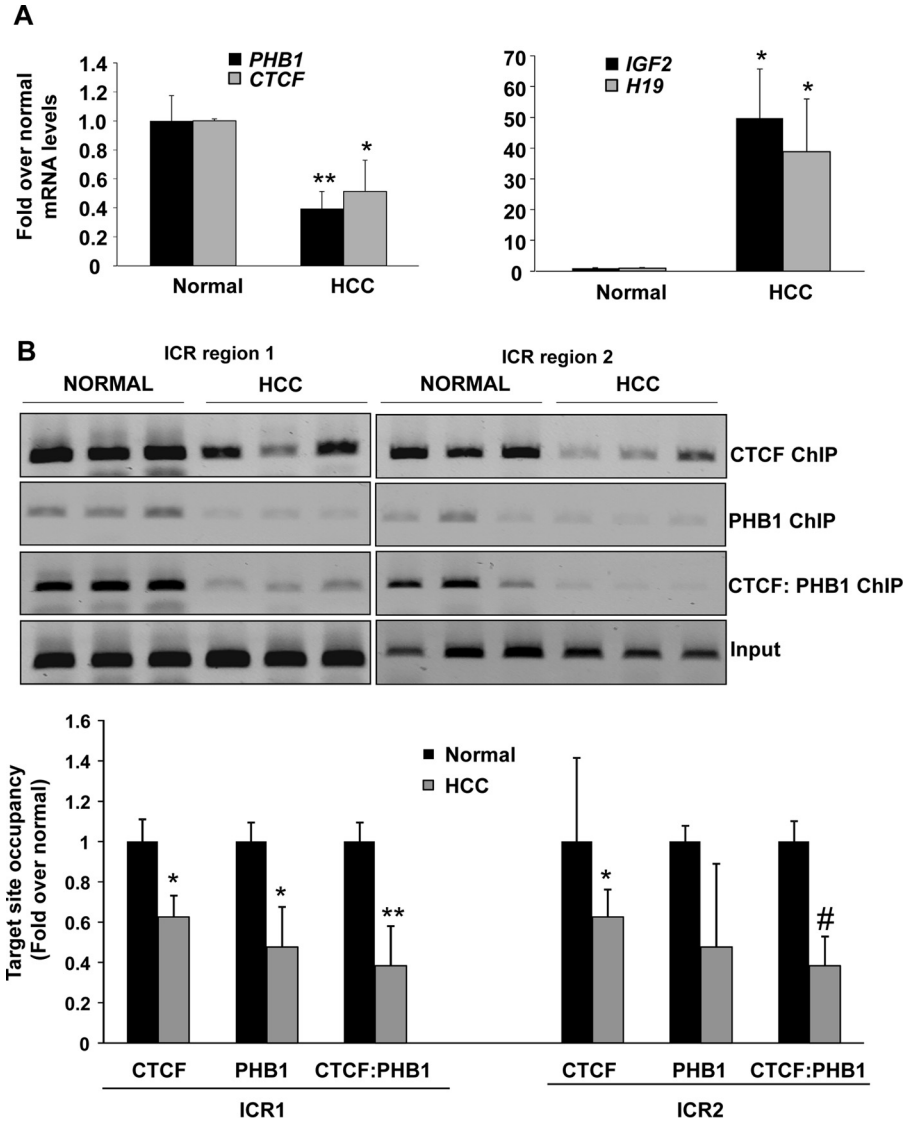

FIGURE 9. **Expression of *IGF2* and *H19* negatively correlates with *PHB1* and *CTCF* expression and ICR binding in human HCC.** *A*, total RNA from normal and HCC tissues was subjected to real-time PCR to measure the relative expression of *PHB1*, *CTCF*, *H19*, and *IGF2*. Results represent mean ± S.E. from 11 HCC and 5 normal livers. *, $p < 0.05$, **, $p < 0.005$ *versus* normal liver. *B*, the co-localization of CTCF and PHB1 on ICR regions 1 and 2 was assessed by ChIP and sequential ChIP of total liver chromatin from normal and HCC tissues as described under "Experimental Procedures." The PCR products were electrophoresed on a 1% agarose gel (*top panel*). The target site occupancy of CTCF and PHB1 on the ICR regions was measured by real-time PCR (*bottom panel*). *, $p < 0.05$, **, $p < 0.005$, #, $p < 0.01$ *versus* normal liver.

3′; ICR2-reverse, 5′-GTCTGCCGAGCAATA-3′. All PCR products were run on 1% agarose gels and stained with SYBR® Green (Thermo Fisher Scientific) for 15–30 min. SYBR® Green-based real-time PCR was performed with the above primers to quantify the target site occupancy of CTCF and PHB1. Real-time PCR Ct values were normalized to that of input DNA according to the formula: target site occupancy $= 2^{-\Delta Ct}$ where ΔCt = Ct of immunoprecipitated DNA − Ct of input DNA. In experiments where the relative binding of CTCF was compared between *Phb1* silencing and negative control groups, the relative target site occupancy $= 2^{-\Delta\Delta Ct}$ where $\Delta\Delta Ct = \Delta Ct$ of knockdown group − ΔCt of negative control group.

EMSA with Antibody Supershift Assay—Nuclear extracts were prepared from AML12 cells according to the NE-PER® nuclear and cytoplasmic extraction protocol (Thermo Fisher Scientific). Extracts were subjected to EMSA following the LightShift® Chemiluminescent EMSA Kit (Thermo Fisher Scientific). Extracts (10 μg) were incubated for 1 h with 1× binding buffer from the kit, 1× PBS, 10% glycerol, 5 mM $MgCl_2$, 1 mM DTT, 50 ng/μl poly(dI·dC), 0.1% NP-40, and 10 fmol of a 3′-biotin-labeled double-stranded oligonucleotide probe containing CTCF-binding sites: 5′-CCGCGTGGCCGCACGGCCCGCGCGGTGGCCGCGTG-3′. Following probe binding, supershift of the probe was performed for 1 h using 3 μg of antibodies that were used in the ChIP assay. The samples were electrophoresed on a 5% acrylamide gel and transferred to a Biodyne™ B Nylon Membrane (Thermo Fisher Scientific). Because the available size of Biodyne™ is restricted to 8 by 12 cm, the probe portion of the gel was transferred using a separate membrane but in the same cassette as the rest of the gel (Fig. 6*B*).

Cell Proliferation Assays—To estimate cell proliferation of SAMe-D cells, cells were plated at a density of 1×10^4 cells/well

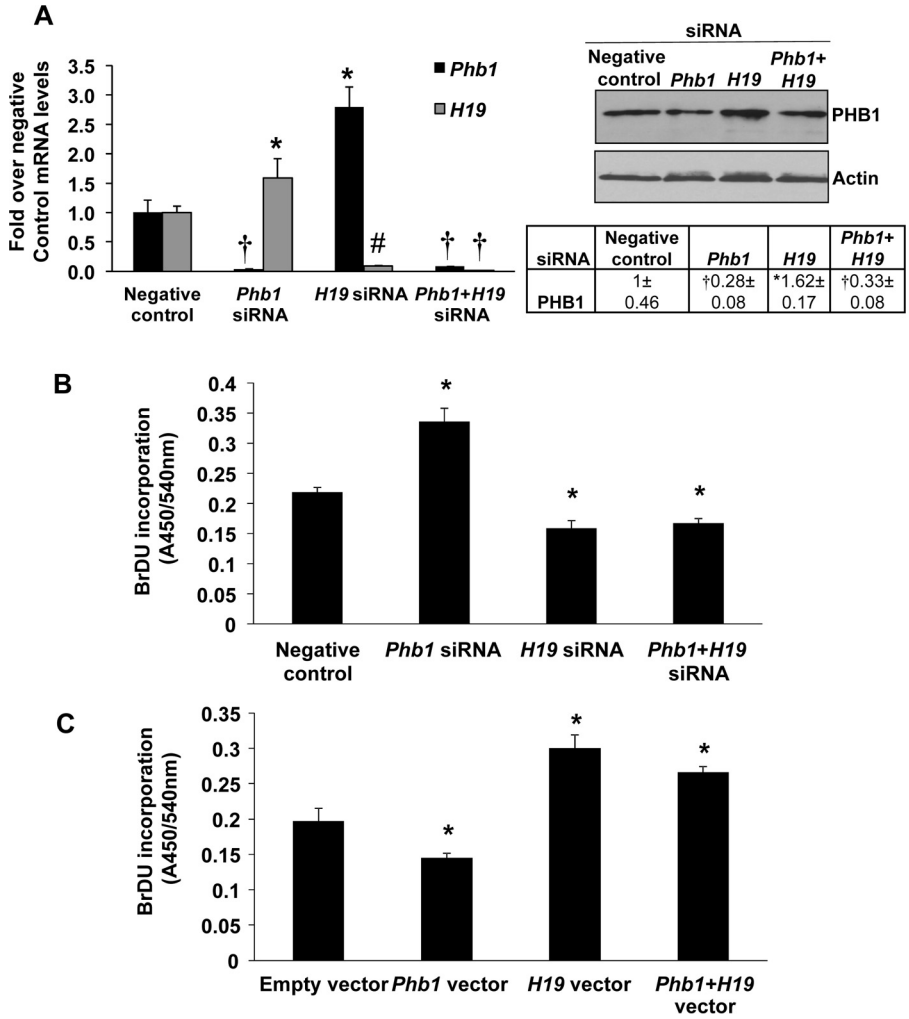

FIGURE 10. **Modulation of *H19* gene influences PHB1-mediated cellular proliferation in liver cancer cells.** *A*, SAMe-D cells were transfected with negative control, *Phb1*, *H19*, or *Phb1*+*H19* siRNA. The effect of *Phb1* and *H19* siRNAs on total mRNA level was evaluated by real-time PCR (*left panel*), and total protein level was estimated by Western blotting for PHB1 (*right panel*). Results represent mean ± S.E. from three experiments. *, $p < 0.05$, #, $p < 0.01$, †, $p < 0.001$ *versus* negative control. *B*, SAMe-D cells were transfected as in *A* in a 96-well plate format. The incorporation of BrDU into DNA of dividing cells was estimated by A_{450} absorbance as described under "Experimental Procedures." Results represent mean ± S.E. from 4 experiments. *, $p < 0.05$ *versus* negative control. *C*, SAMe-D cells were transfected with EV, *Phb1* vector, *H19* vector, or *Phb1*+*H19* vector in a 96-well plate format. The incorporation of BrDU into DNA of dividing cells was estimated by A_{450} absorbance as described under "Experimental Procedures." Results represent mean ± S.E. from 4 experiments. *, $p < 0.05$ *versus* EV.

of a 96-well plate under knockdown or overexpression conditions as described above. BrDU was added to each well at a dilution of 1:2000 during the last 16 h of knockdown, and its incorporation into DNA (a measure of growth) was measured by absorbance at 450 nm/reference 540 nm using the BrDU Cell Proliferation Assay Kit (Calbiochem).

Statistical Analysis—Data are represented as mean ± S.E. from 3–4 experimental groups. Statistical analysis was performed using analysis of variance followed by Student's *t* test. Significance was defined as $p < 0.05$.

Author Contributions—S. C. L. conceived the idea for this work and obtained funding. K. R. and N. M. contributed equally to this work by conducting the experiments and confirming results from Figures 1 and 2. K. S. K. did the initial experiments from Figures 1 and 2. K. R., N. M., and S. L. contributed to analyzing the data and writing the paper. J. M. M. provided scientific input for these studies

References

1. Mishra, S., Murphy, L. C., and Murphy, L. J. (2006) The Prohibitins: emerging roles in diverse functions. *J. Cell. Mol. Med.* **10,** 353–363
2. Nijtmans, L. G., de Jong, L., Artal Sanz, M., Coates, P. J., Berden, J. A., Back, J. W., Muijsers, A. O., van der Spek, H., and Grivell, L. A. (2000) Prohibitins act as a membrane-bound chaperone for the stabilization of mitochondrial proteins. *EMBO J.* **19,** 2444–2451
3. Peng, Y. T., Chen, P., Ouyang, R. Y., and Song, L. (2015) Multifaceted role of prohibitin in cell survival and apoptosis. *Apoptosis* **20,** 1135–1149
4. Zhou, T. B., Qin, Y. H., Lei, F. Y., Huang, W. F., and Drummen, G. P. (2013) Prohibitin is associated with antioxidative protection in hypoxia/reoxygenation-induced renal tubular epithelial cell injury. *Sci. Rep.* **3,** 3123
5. Tatsuta, T., Model, K., and Langer, T. (2005) Formation of membrane-bound ring complexes by prohibitins in mitochondria. *Mol. Biol. Cell* **16,** 248–259
6. Wang, S., Nath, N., Fusaro, G., and Chellappan, S. (1999) Rb and prohibitin target distinct regions of E2F1 for repression and respond to different upstream signals. *Mol. Cell. Biol.* **19,** 7447–7460
7. Wang, S., Fusaro, G., Padmanabhan, J., and Chellappan, S. P. (2002) Prohibitin co-localizes with Rb in the nucleus and recruits N-CoR and HDAC1 for transcriptional repression. *Oncogene* **21,** 8388–8396

8. Fusaro, G., Dasgupta, P., Rastogi, S., Joshi, B., and Chellappan, S. (2003) Prohibitin induces the transcriptional activity of p53 and is exported from the nucleus upon apoptotic signaling. *J. Biol. Chem.* **278,** 47853–47861
9. Theiss, A. L., and Sitaraman, S. V. (2011) The role and therapeutic potential of prohibitin in disease. *Biochim. Biophys. Acta* **1813,** 1137–1143
10. Chowdhury, I., Thompson, W. E., and Thomas, K. (2014) Prohibitins role in cellular survival through Ras-Raf-MEK-ERK pathway. *J. Cell. Physiol.* **229,** 998–1004
11. McClung, J. K., Danner, D. B., Stewart, D. A., Smith, J. R., Schneider, E. L., Lumpkin, C. K., Dell'Orco, R. T., and Nuell, M. J. (1989) Isolation of a cDNA that hybrid selects antiproliferative mRNA from rat liver. *Biochem. Biophys. Res. Commun.* **164,** 1316–1322
12. Ko, K. S., Tomasi, M. L., Iglesias-Ara, A., French, B. A., French, S. W., Ramani, K., Lozano, J. J., Oh, P., He, L., Stiles, B. L., Li, T. W., Yang, H., Martínez-Chantar, M. L., Mato, J. M., and Lu, S. C. (2010) Liver-specific deletion of prohibitin 1 results in spontaneous liver injury, fibrosis, and hepatocellular carcinoma in mice. *Hepatology* **52,** 2096–2108
13. Sasaki, H., Ishihara, K., and Kato, R. (2000) Mechanisms of *Igf2*/*H19* imprinting: DNA methylation, chromatin and long-distance gene regulation. *J. Biochem.* **127,** 711–715
14. Kim, K. S., and Lee, Y. I. (1997) Biallelic expression of the *H19* and *IGF2* genes in hepatocellular carcinoma. *Cancer Lett.* **119,** 143–148
15. Vernucci, M., Cerrato, F., Besnard, N., Casola, S., Pedone, P. V., Bruni, C. B., and Riccio, A. (2000) The *H19* endodermal enhancer is required for *Igf2* activation and tumor formation in experimental liver carcinogenesis. *Oncogene* **19,** 6376–6385
16. Toretsky, J. A., and Helman, L. J. (1996) Involvement of IGF-II in human cancer. *J. Endocrinol.* **149,** 367–372
17. Nussbaum, T., Samarin, J., Ehemann, V., Bissinger, M., Ryschich, E., Khamidjanov, A., Yu, X., Gretz, N., Schirmacher, P., and Breuhahn, K. (2008) Autocrine insulin-like growth factor-II stimulation of tumor cell migration is a progression step in human hepatocarcinogenesis. *Hepatology* **48,** 146–156
18. Yamamoto, Y., Nishikawa, Y., Tokairin, T., Omori, Y., and Enomoto, K. (2004) Increased expression of H19 non-coding mRNA follows hepatocyte proliferation in the rat and mouse. *J. Hepatol.* **40,** 808–814
19. Matouk, I. J., DeGroot, N., Mezan, S., Ayesh, S., Abu-lail, R., Hochberg, A., and Galun, E. (2007) The H19 non-coding RNA is essential for human tumor growth. *PLoS ONE* **2,** e845
20. Kurukuti, S., Tiwari, V. K., Tavoosidana, G., Pugacheva, E., Murrell, A., Zhao, Z., Lobanenkov, V., Reik, W., and Ohlsson, R. (2006) CTCF binding at the *H19* imprinting control region mediates maternally inherited higher-order chromatin conformation to restrict enhancer access to *Igf2*. *Proc. Natl. Acad. Sci. U.S.A.* **103,** 10684–10689
21. Martínez-López, N., Varela-Rey, M., Fernández-Ramos, D., Woodhoo, A., Vázquez-Chantada, M., Embade, N., Espinosa-Hevia, L., Bustamante, F. J., Parada, L. A., Rodriguez, M. S., Lu, S. C., Mato, J. M., and Martínez-Chantar, M. L. (2010) Activation of LKB1-Akt pathway independent of phosphoinositide 3-kinase plays a critical role in the proliferation of hepatocellular carcinoma from nonalcoholic steatohepatitis. *Hepatology* **52,** 1621–1631
22. Sánchez-Quiles, V., Segura, V., Bigaud, E., He, B., O'Malley, B. W., Santamaría, E., Prieto, J., and Corrales, F. J. (2012) Prohibitin-1 deficiency promotes inflammation and increases sensitivity to liver injury. *J. Proteomics* **75,** 5783–5792
23. Hark, A. T., Schoenherr, C. J., Katz, D. J., Ingram, R. S., Levorse, J. M., and Tilghman, S. M. (2000) CTCF mediates methylation-sensitive enhancer-blocking activity at the *H19*/*Igf2* locus. *Nature* **405,** 486–489
24. Thorvaldsen, J. L., Mann, M. R., Nwoko, O., Duran, K. L., and Bartolomei, M. S. (2002) Analysis of sequence upstream of the endogenous *H19* gene reveals elements both essential and dispensable for imprinting. *Mol. Cell. Biol.* **22,** 2450–2462
25. Bayoumi, A. S., Sayed, A., Broskova, Z., Teoh, J. P., Wilson, J., Su, H., Tang, Y. L., and Kim, I. M. (2016) Crosstalk between long noncoding RNAs and microRNAs in health and disease. *Int. J. Mol. Sci.* **17,**
26. Ramani, K., Donoyan, S., Tomasi, M. L., and Park, S. (2015) Role of methionine adenosyltransferase α2 and β phosphorylation and stabilization in human hepatic stellate cell trans-differentiation. *J. Cell. Physiol.* **230,** 1075–1085

Prohibitin 1 Regulates the H19-Igf2 Axis and Proliferation in Hepatocytes

Komal Ramani, Nirmala Mavila, Kwang Suk Ko, José M. Mato and Shelly C. Lu

J. Biol. Chem. 2016, 291:24148-24159.
doi: 10.1074/jbc.M116.744045 originally published online September 29, 2016